Electronic Supplementary Material (ESI) for Reaction Chemistry & Engineering.


**Supplementary Information**

# Direct Observation of the Kinetics of Gas-Solid Reactions using In-situ Kinetic and Spectroscopic Techniques

*Adam S. Hoffman*[b,†], *Sara Azzam*[a,†], *Kai Zhang*[b,c,†], *Yahong Xu*[b], *Yijin Liu*[b,*], *Simon R. Bare*[b,*], *Dante A. Simonetti*[a,*]

[a] Chemical and Biomolecular Engineering Department, University of California-Los Angeles, Los Angeles, CA 90095

[b] Stanford Synchrotron Radiation Lightsource, SLAC National Accelerator Laboratory, Menlo Park, CA 94025

[c] Beijing Synchrotron Radiation Facility, Institute of High Energy Physics, Chinese Academy of Sciences, Beijing 100049, China

*D. A. S.: E-mail: dasimonetti@ucla.edu
*Y. L.: E-mail: liuyijin@slac.stanford.edu
*S. R. B.: E-mail: srbare@slac.stanford.edu

**Extended Data and Discussion**

*Scanning Electron Microscopy*

The commercially produced CuO-based sample used in this study (HiFuel W230 denoted at CuO-1) is a formed cylindrical extrudate. For the sorption experiments in this work, the extrudates were crushed and sieved into a narrow range of agglomerate sizes for fixed bed experiments (+200-100 mesh; 75-125 μm sized particles) and into fine powders (-270 mesh) of ~20 μm particles for XAS and TXM experiments. Figure S1A shows the topological features of the representative particles studied in the XAS and TXM experiments. Figure S1B-C shows SEM images of ~75 μm sized HiFuel agglomerates before and after sulfidation in a fixed bed experiment. The laboratory CuO sample (denoted as CuO-2) is prepared as a powder consisting of various agglomerate sizes. The as-prepared sample was sieved and the +200-100 mesh fraction was used for fixed bed studies with the fine powder fraction (-270 mesh) used in XAS and TXM experiments. Figure S2 shows SEM images of the CuO-2 sample (-270 mesh) before and after sulfidation at magnifications that show the morphological and topographical features.

Figure S1B-C shows no apparent structural changes upon sulfidation of CuO-1 indicating that the presence of the $Al_2O_3$ and ZnO provides a binding matrix that prevents the collapse of the structures after the conversion of copper oxide to copper sulfide. The lack of a supporting matrix in the nanoparticles, CuO-2 (Figure S2A), results in a collapse of the spherical particles into flakes of partially sulfided copper (II) oxide (Figure S2B).

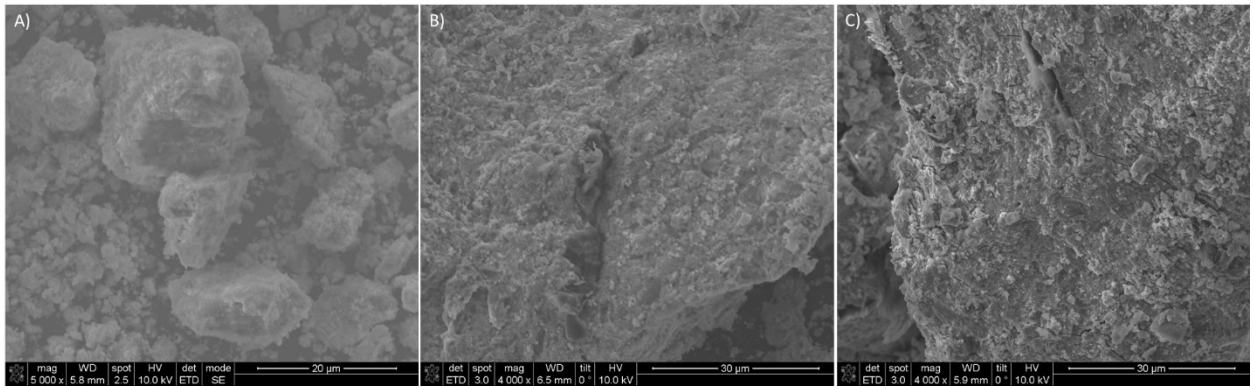


**Figure S1**: SEM images of HiFuel W230, CuO-1, A) -270 mesh (>53 μm) particles before sulfidation, B) +200-100 mesh (75-125 μm particles) before sulfidation, and B) +200-100 mesh (75-125 μm particles) after reaction with 110 $cm^3$(STP) $min^{-1}$ of 930 ppm $H_2S/N_2$ at ambient temperature (294 K) and pressure (1.1 atm).

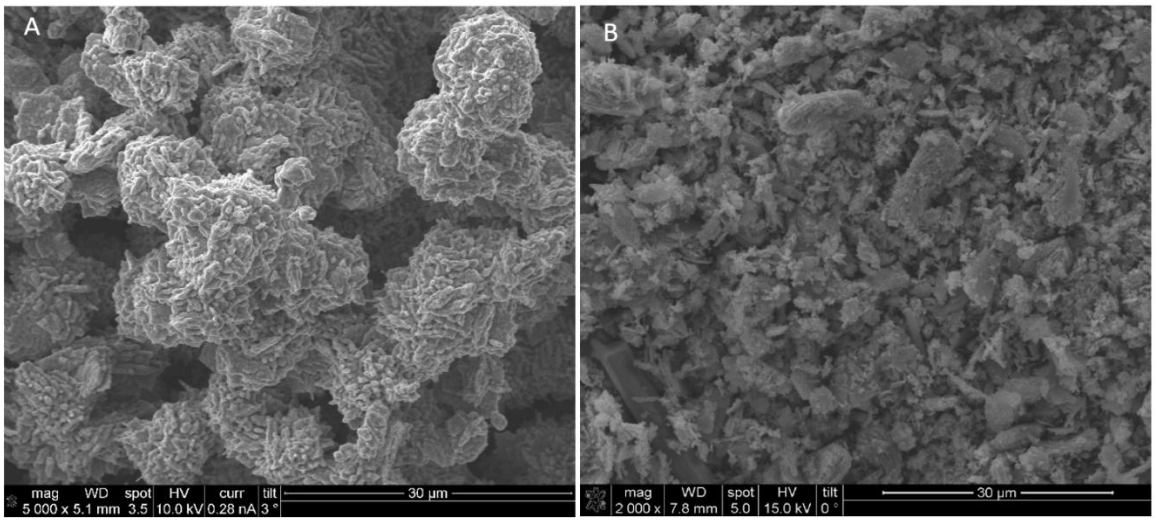


**Figure S2:** SEM images of copper (II) oxide nanoparticles prepared by precipitation from copper (II) nitrate trihydrate precursor, CuO-2, A) before sulfidation and B) after reaction with 84 $cm^3$(STP) $min^{-1}$ of 1000 ppm $H_2S/N_2$ at ambient temperature (294 K) and pressure (1.1 atm).

*X-ray Diffraction*

Figures S3-S4 present the diffraction patterns for fresh and spent adsorbents. The peaks at $2\theta = 35.7°$ and 38.9° in Figures S3 (red) and S4 (red) correspond to the (002) and (111) planes of copper (II) oxide, respectively. The diffraction pattern of CuO-1 (red line in Figure S3) consists of broad peaks, and analysis of the $2\theta = 38.9°$ peak using the Scherrer equation indicates 2.8 nm-sized CuO crystallites. The CuO-2 diffraction pattern (red line in Figure S4) shows sharp peaks

that indicate higher degrees of crystallinity (47 nm and 23 nm CuO crystallites via analysis of the $2\theta = 35.7^{o}$ and $38.9^{o}$ peaks, respectively, using the Scherrer equation). Figures S3 (blue) and S4 (blue) show broadening in the copper (II) oxide peaks after the sulfidation. This broadening is more pronounced for CuO-2 (decrease in CuO crystallite size from 23 to 11 nm) compared to CuO-1 (negligible decrease in CuO crystallite size from 2.8 to 2.3 nm). The loss of CuO crystallinity upon sulfidation of CuO-2 is consistent with the change in the particle shape and size observed via SEM of the sulfided CuO-2 sample (Figure S2B) and indicates the breakdown of crystalline CuO upon reaction with sulfur as a result of the volume expansion going from CuO to CuS.

A peak at $2\theta = 48°$ is observed in the pattern of the sulfided CuO-2 sample, which corresponds to the (110) plane of hexagonal copper (II) sulfide and indicates the formation of CuS as the predominant reaction product. The absence of copper sulfide peaks in the pattern of CuO-1 after reaction indicates amorphous copper sulfide phases or copper sulfide with crystallite sizes below the limit of detection with XRD.

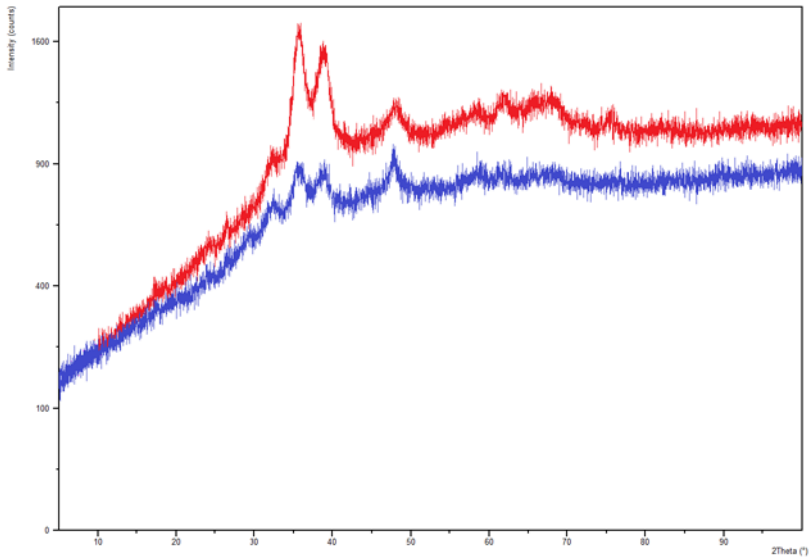


**Figure S3:** Diffraction patterns of CuO-1 before (red) and after (blue) sulfidation with 110 $cm^3$(STP) $min^{-1}$ of 930 ppm $H_2S/N_2$ at ambient temperature (294 K) and pressure (1.1 atm).

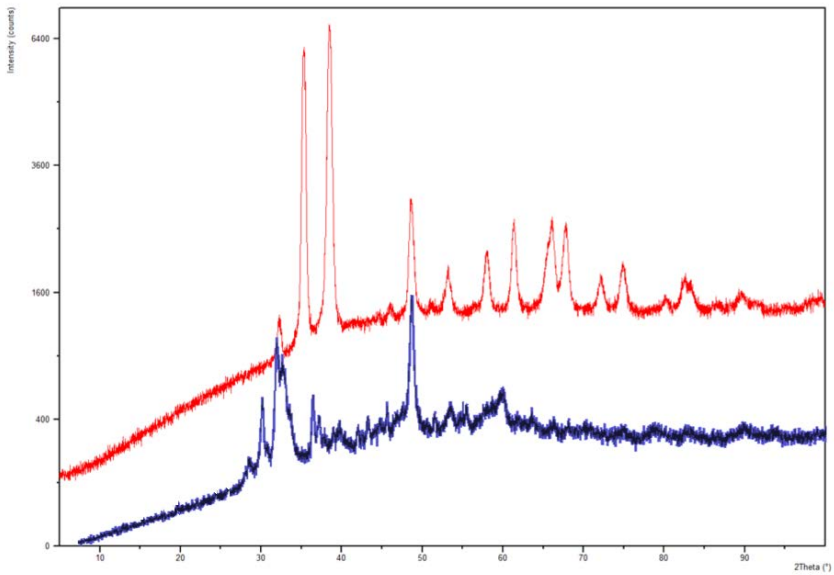


**Figure S4:** Diffraction patterns of CuO-2 before (red) and after (blue) sulfidation with 84 $cm^3$(STP) $min^{-1}$ of 1000 ppm $H_2S/N_2$ at ambient temperature (294 K) and pressure (1.1 atm).

**Porosity Measurements**

Table S1 shows pore volumes (BJH method) and surface areas (BET method) determined from $N_2$ physisorption isotherms. The fresh materials have similar surface areas and total pore volumes. HiFuel W230, CuO-1, exhibited a 3.8-fold decrease in surface area and a 2.7-fold decrease in pore volume after reaction with $H_2S$. The CuO nanoparticles, CuO-2, exhibited only a 60% decrease in pore volume with a 50% increase in surface area.

**Table S1:** Pore volumes and BET surface areas of fresh and sulfided CuO-based sorbents.

| Adsorbent | Fresh pore volume ($cm^3/g$) | Fresh surface area ($m^2/g$) | Spent pore volume ($cm^3/g$) | Spent surface area ($m^2/g$) |
|---|---|---|---|---|
| HiFuel W230 (CuO-1) | 0.14 | 63 | 0.051 | 18 |
| CuO (CuO-2) | 0.17 | 59 | 0.11 | 87 |

**Sorption Experiments**

*Fixed bed experiments*

The breakthrough curve data (Figure 2 of main text) was analyzed using the linear driving force model derived by Cooper[3] (see Model Derivation section below) to determine sorption rate parameters (kK). These rate parameters consist of contributions from bulk and pore diffusion which can be determined using known engineering correlations (described in the Model Derivation section below). Table S2 shows the k values regressed from the experimental data and the values of bulk and pore diffusion resistances. The sum of the reciprocals of these kK values reveals that the experimental kK primarily reflects reaction-diffusion phenomena because resistance from pore and bulk phase diffusion is small.

**Table S2:** Rate parameters for the Cooper model (k; determined from data in Figure 3 of main text) along with the theoretical values for interpellet and intrapellet mass transfer resistances.

| Adsorbent | kK ($s^{-1}$) | $k_{interpellet}$ ($s^{-1}$) | $k_{pores}$ ($s^{-1}$) | $k_{rxn}$ ($s^{-1}$) |
|---|---|---|---|---|
| HiFuel W230 CuO-1 | 5.2 ± 0.4 | 22000 | 260 | 5.3 |
| CuO CuO-2 | 6.1 ± 0.2 | 7400 | 90 | 6.5 |

The Cooper model and the rate parameters listed in Table S2 were used to simulate the concentration profiles from the effluent of the *in-situ* XAS and TXM reactors to confirm the absence of axial concentration gradients. These reactors consisted of a ¼ inch OD glassy carbon tube containing approximately 50 mg of adsorbent diluted with 100 mg of boron nitride (XAS) and a 500 μm quartz capillary with less than 1 mg of adsorbent (TXM). Table S3 shows that the calculated time required for the effluent and inlet concentrations to be the same for typical conditions (50 mL/min of 1000 ppm $H_2S$ feed at 294 K and 1 atm) are less than 30 minutes, indicating that the *in-situ* XAS and TXM data discussed in the main text were collected under a constant atmosphere of $H_2S$ in He.

**Table S3:** Time to reach equal concentrations of $H_2S$ in effluent and inlet streams for *in-situ* XAS and TXM reactors. Reaction conditions were 50 mL/min of 1000 ppm $H_2S$ feed at ambient temperature and pressure.

| Sample | Capacity (wt%) | Reactor | Time for complete breakthrough (min)[a] |
|---|---|---|---|
| CuO-1 | 12 | XAS | 30 |
| CuO-2 | 6 | XAS | 15 |
| CuO-1 | 12 | TXM | Immediate |
| CuO-2 | 6 | TXM | Immediate |

[a] Determined using the model derived by Cooper[1] and the parameters in Tables S1-S2

*Analysis of heat transfer effects*

The intra-particle heat transfer criterion (Equation S1) was determined for these experiments to prove the absence of intra-particle temperature gradients[5].

$$\frac{|\Delta H| r''' r_p^2}{\lambda T_s} < \frac{0.75 E_a T_s}{R} \quad \text{(S1)}$$

The initial rate of reaction ($r'''$) was determined from the data in Figure 4 of the main text (1.5 and 0.33 mol $m^{-3}$ $s^{-1}$ for CuO-1 and CuO-2, respectively). The heat of reaction (ΔH) for CuO sulfidation by gas phase $H_2S$ is 117 kJ $mol^{-1}$ and an activation energy ($E_a$) of 21 kJ $mol^{-1}$ was used. The thermal conductivity (λ) for CuO (0.033 kW $m^{-1}$ $K^{-1}$) was used for sample CuO-1, and a mass based linear combination of CuO and ZnO (0.050 kW $m^{-1}$ $K^{-1}$) was used for the thermal conductivity of sample CuO-2. Since the reaction was conducted at ambient conditions, the surface temperature ($T_s$) was taken to be ambient temperature (297 K). These parameter values provide upper limits for the intra-particle heat transfer criterion of 3.4 x $10^{-9}$ for CuO-1 and 3.9 x $10^{-10}$ for CuO-2, which are much less than the maximum limit of 4.4 x $10^{-4}$. These values indicate the absence of temperature gradients from the heat generated via reaction.

*Kinetic Analysis of in-situ XAS Data*

Figures 4 and 6 in the main text shows the model fit to the conversion data derived from the XAS and TXM experiments. The parameter values and confidence intervals are listed in Table S4.

**Table S4:** Random pore model parameters with 95% confidence intervals derived from in-situ bulk XAS measurements for CuO-1 and CuO-2 (Figure 4 in main text).

| Sample | k x $10^3$ ($cm^4$ $mol^{-1}$ $s^{-1}$) | D x $10^{12}$ ($cm^2$ $s^{-1}$) |
|---|---|---|
| CuO-2 | 8.4 ± 2.6 | 2.0 ± 0.2 |
| CuO-1 | 5.6 ± 0.9 | 1.1 ± 0.1 |

**Table S5:** Random pore model parameters with 95% confidence intervals (CI) at various radial positions derived from in-situ bulk TXM-XAS measurements for CuO-2 (Figure 6 in main text).

| Fractional Distance | k x $10^3$ ($cm^4$ $mol^{-1}$ $s^{-1}$) | 95% CI | D x $10^{12}$ ($cm^2$ $s^{-1}$) | 95% CI |
|---|---|---|---|---|
| 0.01 | 0.39 | 0.05 | 7.25 | 1.02 |
| 0.11 | 0.42 | 0.05 | 5.00 | 1.64 |
| 0.21 | 0.22 | 0.05 | 10.83 | 2.12 |
| 0.31 | 0.20 | 0.08 | 7.89 | 2.58 |
| 0.41 | 0.15 | 0.05 | 10.61 | 1.95 |
| 0.5 | 0.12 | 0.04 | 11.17 | 1.77 |
| 0.61 | 0.10 | 0.05 | 14.42 | 2.34 |
| 0.71 | 0.07 | 0.09 | 13.97 | 4.14 |

*Linear Combination Fitting Analysis of XANES Spectra*

Athena was used for the linear combination fitting of the XANES spectra characterizing the sulfidation of the copper oxide. XANES spectra were fit using normalized spectra over a range from -30 eV to 50 eV above the edge energy. The contributions of all standards were forced such that the weight of each contribution was restricted to a value between 0 and 1. XANES spectra of CuO and CuS were used as standards in the linear combination fitting. An example of the sulfidation of sample CuO-1 as it was exposed to flowing 1000 ppm $H_2S$ in helium at room temperature and atmospheric pressure is shown in Figure S5.

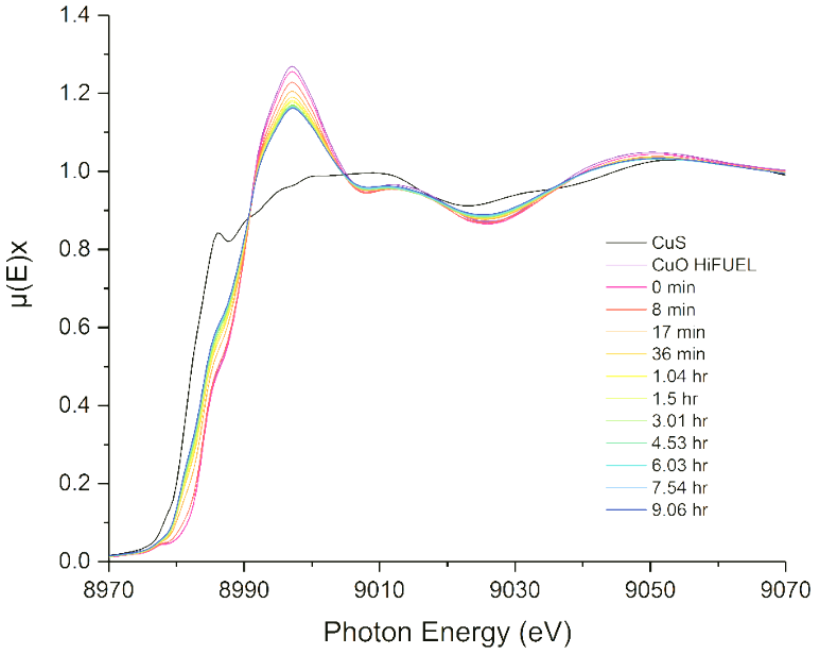


**Figure S5.** Time resolved bulk XANES spectra of CuO-1 as it is exposed to flowing 1000 ppm $H_2S$ in helium at room temperature and atmospheric pressure. Copper (II) sulfide, dark green, is included for reference.

**EXAFS Analysis of Cu Metal Foil and Initial State of CuO Samples**

FEFF 6 was used to determine the scattering paths in the EXAFS analysis based upon CIF files (from the Inorganic Crystal Structure Database (ICSD)[2]) of bulk copper compounds (*fcc*-Cu metal (ICSD 53247), and CuO (ICSD 16025)). The amplitude reduction factor, $S_0^2$, was determined to be 0.81 by modeling of bulk Cu.

The best-fit model parameters for each sample are given in Table S6, with the model compared to the data for CuO-1 and CuO-2 in Figures S6 and S7, respectively. Due to the complexity and large number of scattering paths in CuO, the models were simplified using the following: (i) only single-scattering paths; (ii) coordination numbers, N, scale linearly by a factor $\alpha$; (iii) "like" scattering paths have the same $\sigma^2$ values.

**Table S6.** Summary of the EXAFS fit parameters[a] characterizing the initial CuO samples. The EXAFS data was collected at room temperature in flowing helium.

| Sample | Absorber-Backscatter Scattering Path | *N* | $10^3$ x $\sigma^2$ (Å$^2$) | *R* (Å) | $\Delta E_0$ (eV) | *k*-range (Å$^{-1}$) | *R*-range (Å) |
|---|---|---|---|---|---|---|---|
| CuO-1 | Cu-O | 2.7 ± 0.3 | 1.8 ± 1.7 | 1.96 ± 0.01 | 1.7 ± 1.7 | 3.0-11.0 | 1.1-3.2 |
| | Cu-O | 1.3 ± 0.2 | 1.8 ± 1.7 | 2.82 ± 0.08 | | | |
| | Cu-Cu | 2.7 ± 0.3 | 6.7 ± 6.2 | 2.96 ± 0.03 | | | |
| | Cu-Cu | 2.7 ± 0.3 | 6.7 ± 6.2 | 3.16 ± 0.05 | | | |
| | Cu-Cu | 1.3 ± 0.2 | 6.7 ± 6.2 | 3.38 ± 0.08 | | | |
| CuO-2 | Cu-O | 3.4 ± 4.3 | 2.2 ± 14.6 | 1.96 ± 0.10 | 7.10 ± 13.0 | 3.0-11.0 | 0.9-3.2 |
| | Cu-O | 1.7 ± 2.2 | 2.3 ± 14.6 | 2.78 ± 0.57 | | | |
| | Cu-Cu | 3.4 ± 4.3 | 4.2 ± 17.8 | 2.90 ± 0.21 | | | |
| | Cu-Cu | 3.4 ± 4.3 | 4.2 ± 17.8 | 3.08 ± 0.23 | | | |
| | Cu-Cu | 1.7 ± 2.2 | 4.2 ± 17.8 | 3.17 ± 0.28 | | | |

[a] Notation: $S_0^2$, amplitude reduction factor, *N*, coordination number, $\sigma^2$, disorder term (Debye-Waller factor), *R*, distance between absorber and backscatter, $\Delta E_0$, energy correction term.

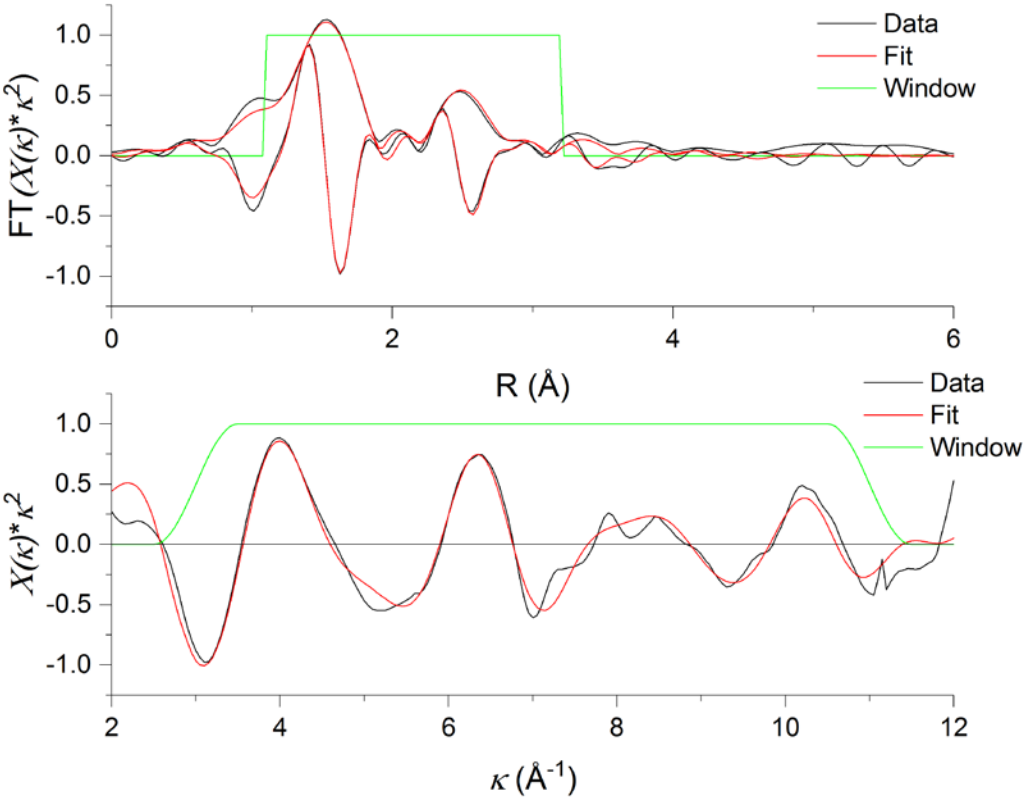


**Figure S6.** EXAFS data and best-fit model characterizing the initial state of the commercial CuO sample, CuO-1. Spectra were collected at room temperature in flowing helium. **Top**: $k^2$-weighted magnitude and imaginary part of the Fourier transform of the data (black line) and fit (red line). **Bottom**: $k^2$-weighted EXAFS function of the data (black line) and fit (red line). The green line in both plots represents the window used to determine the number if independent parameters.

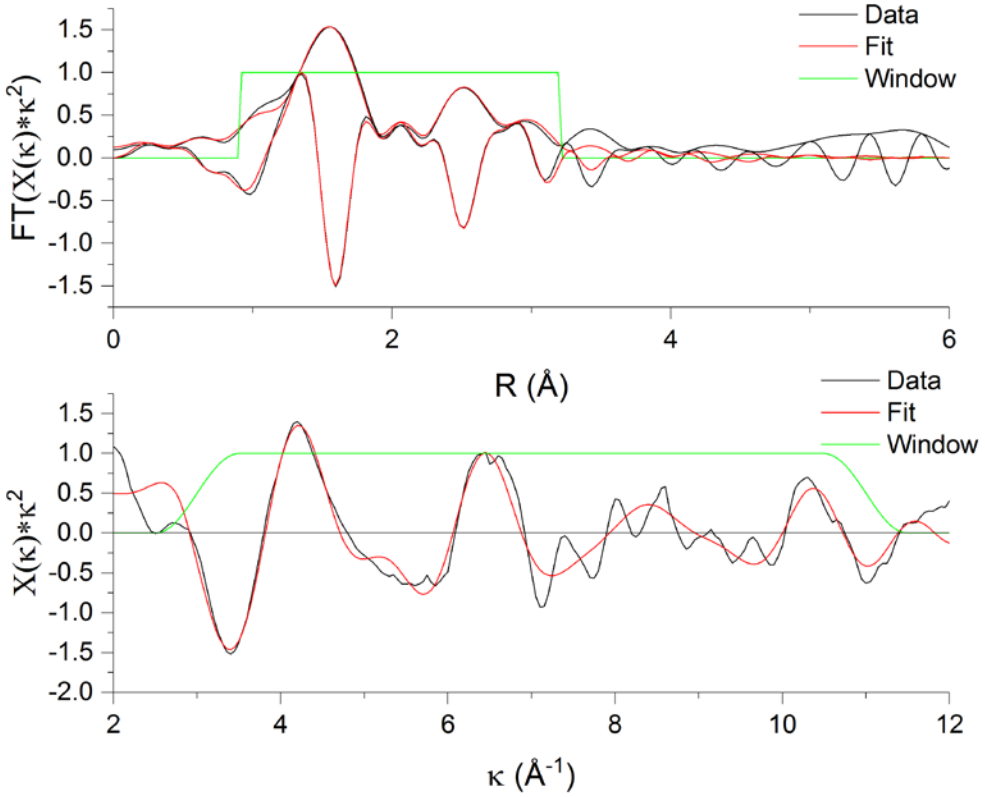


**Figure S7.** EXAFS data and best-fit model characterizing the initial state of the CuO nanoparticle sample, CuO-2. Spectra were collected at room temperature in flowing helium. **Top**: $k^2$-weighted magnitude and imaginary part of the Fourier transform of the data (black line) and fit (red line). **Bottom**: $k^2$-weighted EXAFS function of the data (black line) and fit (red line). The green line in both plots represents the window used to determine the number if independent parameters.

## Model Derivation

*Linear Driving Force Model for Fixed Bed Sorption*

Reactive sorption of $H_2S$ from a gaseous stream can be described by the mass balance across a differential element of the bed as follows[3]:

$$v\left(\frac{\delta C}{\delta Z}\right)_t + \left(\frac{\delta C}{\delta t}\right)_z + \frac{1-\varepsilon}{\varepsilon} \cdot \left(\frac{\delta q}{\delta t}\right)_z = 0 \qquad S2$$

where $v$ is the axial interstitial velocity of fluid, $z$ is the axial distance coordinate in the direction of the flow, $C$ is the concentration of the contaminant in the bulk fluid, $t$ is time, $\varepsilon$ is bed void fraction and $q$ is the average concentration of solute in the solid adsorbent (capacity). To solve

this equation for the concentration profile, Cooper applied a linear driving force equation where the overall adsorption rate is described as[1]

$$\frac{\delta q}{\delta t} = k(q_s - q) \qquad S3$$

where k is the adsorption rate parameter. The analytical solution of the coupled PDE-ODE system (Equations S4-S6) is a piece-wise solution:

$$\frac{C}{C_0} = 1 - \text{ʒ}e^{-\tau}, \qquad \text{ʒ} \leq 1 \qquad S4$$

$$\frac{C}{C_0} = 1 - e^{\text{ʒ}-\tau-1}, 1 \leq \text{ʒ} \leq 1 + \tau \qquad S5$$

$$\frac{C}{C_0} = 0, \text{ʒ} \geq 1 + \tau \qquad S6$$

where $\tau = k[t - \frac{x}{v}]$ and $\text{ʒ} = (\frac{kq_s x}{C_0 v})(\frac{(1-\varepsilon)}{\varepsilon})$ are dimensionless time and axial distance, respectively. This solution is a two parameter model (the sorption rate parameter (k) and the maximum saturation capacity ($q_s$)) that relates the properties of the material and the experimental conditions to the concentration-time profile (breakthrough curve) of the contaminant in the effluent of the reactor. If the saturation capacity is experimentally measured, then the model reduces to a single parameter (k).

The total resistance to $H_2S$ uptake (kK) consists of contributions to the overall sorption rate from (i) diffusion in the bulk fluid, (ii) diffusion in the pores of the solid, and (iii) reaction/diffusion phenomena occurring at the surface of the reactive phase according to Equation S7[3,4]

$$\frac{1}{kK} = \frac{R_p}{3k_f} + \frac{R_p^2}{15\varepsilon_p D_p} + \frac{1}{k_{rxn}} \qquad S7$$

where $R_p$ is the radius of the agglomerates of the solid phase, $D_p$ is the diffusivity of the contaminant within the pores of the solid, $k_f$ is the fluid film mass transfer coefficient, K is the ratio of the maximum $H_2S$ capacity of the solid to the inlet gas phase $H_2S$ concentration, and $\varepsilon_p$ is the porosity of the solid particles. In these studies, the value of $k_f$ was determined using the equation for the Sherwood number (Equation S8) in which $D_M$ is the molecular diffusivity of the contaminant molecule in the bulk fluid (calculated for gases using the Chapman-Enskog equation[4]; Equation S9), Sc is the Schmidt number, and Re is the Reynolds number[3,5,6]

$$k_f = \frac{D_M Sh}{2R_p} \qquad Sh = 2 + 1.1Sc^{1/3}Re^{0.6} \qquad S8$$

$$D_M = \frac{0.00266T^{3/2}}{PM_{AB}^{1/2}\sigma_{AB}^2\Omega_D} \qquad S9$$

The contribution from pore diffusion was determined by calculating the value for $D_p$ from the sum of diffusion in the macro- and mesopores of the solid according to

$$D_p = \frac{D}{\tau} \qquad \frac{1}{D} = \frac{1}{D_M} + \frac{1}{D_K} \qquad S10$$

where $D_K$ is the Knudsen diffusivity given by $D_K = 9700r(\frac{T}{M})^{1/2}$ (r is the pore radius, T is temperature, and M is the molecular weight of the diffusing species) and $\tau$ is the tortuosity (assumed to be 3 for spherical agglomerates). The reaction rate parameter (k) in Equation S3 can be determined by dividing the overall resistance (determined from the data) by K. When the terms for pore and bulk resistances in Equation S7 are small, then k represents the $k_{rxn}$ which contains contributions from the rate of reaction at the solid surface and diffusion of molecules/atoms through solid reactant/product phases.

*Random Pore Model for Analysis of in-situ XAS Data*

The Random Pore Model (RPM) was used to analyze the conversion versus time data collected from the in-situ XAS studies. A detailed derivation of the model is contained in reference 7. Briefly, the model assumes that the pores are cylindrical and are not created nor destroyed, an expression encompassing both the kinetically controlled and the diffusion controlled regimes can be written as follows:

$$\frac{dX}{dt} = \frac{k_{RPM} S_0 C_b (1-X)\sqrt{1-\Psi ln(1-X)}}{(1-\varepsilon_0)[1+\beta Z/\Psi(\sqrt{1-\Psi ln\,(1-X)}-1]} \qquad S11$$

The Z term is the ratio of the molar volume of the product to the molar volume of the reactants (0.63 for CuS and CuO). The β term represents a modified Biot number that encompasses the rate constant and the effective product layer diffusivity of the system at hand. For a stoichiometrically balanced equation, such as the sulfidation of CuO, this Biot number can be expressed as

$$\beta = \frac{2k_{RPM}(1-\varepsilon_0)}{V_{CuO} D_{RPM} S_0} \qquad S12$$

The parameter Ψ is a function of three structural parameters that can be calculated from a pore size distribution of the material. These parameters are the initial surface area of reaction ($S_0$), the initial total length of pore structure ($L_0$), and the initial porosity ($\varepsilon_0$). Ψ can be calculated as follows:

$$\Psi = \frac{4\pi L_0 (1-\varepsilon_0)}{S_0^2} \qquad S13$$

In the kinetic region, the modified Biot number tends to 0, and in the diffusion region, the modified Biot number tends to infinity. Applying this to Equation S11, and then integrating and simplifying the resulting equation allows for the creation of two distinct functions relating conversion and time:

$$\frac{1}{\Psi}[\sqrt{1-\Psi ln\,(1-X)}-1]=\frac{k_{RPM}S_0(C_b-C_e)t}{2(1-\varepsilon_0)} \qquad S14$$

$$\frac{1}{\Psi}[\sqrt{1-\Psi ln\,(1-X)}-1]=\frac{S_0}{1-\varepsilon_0}\sqrt{\frac{D_{RPM}M_{CuO}C_b t}{2\rho_{CuO}Z}} \qquad S15$$

The left-hand sides of Equations S14-S15 represent a modified conversion which is a simple algebraic relation to the parameters $k_{RPM}$ and $D_{RPM}$. In the kinetically controlled region, the modified conversion is linearly proportional to time, while in the diffusion limited case, modified conversion has a square root of time dependence. Equations S14 and S15 were used to regress the experimental data and determine the kinetic rate constants and diffusivities of the copper oxide samples.

**Data Processing and Analysis**

The Demeter package[8] was used to process and analyze the XAS data. Athena was used to calibrate, align, and normalize all XAS spectra, to average XAS scans, and to extract the χ(k) data used in the EXAFS modeling. Artemis was used for the EXAFS modeling. The X-ray energy of each XAS spectrum was calibrated to the first inflection point of the Cu K-edge of the Cu foil, 8979.0 eV, collected simultaneously. The pre-edge was approximated as a second-order polynomial, and the background was approximated with a cubic-spline. Data were normalized by subtracting a pre-edge and normalizing to an edge-jump of 1.

*Linear Combination Fitting Analysis of XANES Spectra and TXM Data Processing*

Athena was used for the linear combination fitting of the XANES spectra characterizing the sulfidation of the copper oxide. XANES spectra were fit using normalized spectra over a range from -30 eV to 50 eV above the edge energy. The contributions of all standards were forced such that the weight of each contribution was restricted to a value between 0 and 1. XANES spectra of CuO and CuS were used as standards in the linear combination fitting.

*TXM Data Processing*

The TXM data reduction was conducted using an in-house developed software package known as TXM-Wizard[9]. We first used the difference between the images acquired above and below the Cu absorption edge to generate an "edge jump map", which is then used to reject pixels with insufficient absorption signal. After that, the spectra over every individual pixel are normalized separately using a well-established method[10]. We performed linear combination fitting of all the pixel XANES using the standard spectra of CuO and CuS (Figure S5). Two dimensional chemical maps are generated based on the fitting results. The chemical maps in Figure 4A of the main text are color coded to the local chemical compositions based on the similarities of the local Cu XANES spectra that associate with each of the pixels at ~35×35 $nm^2$ to the standard spectra of the known end chemical compositions. The sample slightly drifted during the measurement. As a result, we did not capture the entire particle throughout the experiment. However, the common area in the chemical maps covers a significant portion of the larger particle in Figure 5 of the main text and the entire particle (10 μm) in Figure 5 of the main text (except for the map of the initial state, which is known to be pure CuO (purely red)) and is, therefore, sufficient for further quantification in this work.

**References**


(1) Cooper, R. S. Slow Particle Diffusion in Ion Exchange Columns. *J. Indus. & Eng. Chem. Fund.* **1965**, *4*, 308-313.

(2) ICSD – the Inorganic Crystal Structure Database. The Information Service for Inorganic Crystal Structures. https://www.fiz-karlsruhe.de/de/leistungen/kristallographie/icsd.html (accessed November, 2017).

(3) Ruthven, D. M. *Principles of Adsorption and Adsorption Processes*; Wiley-Interscience: Hoboken, NJ, 1984; pp 62-122.

(4) Dunne, S. R. Industrial Gas Separation Processes. In *Zeolites in Industrial Separation and Catalysis;* Kulprathipanja, S., Eds.; Wiley-VCH: Weinheim, Germany, 2010; pp 273-304.

(5) Stewart, W. E., and Caracotsios, M. *Computer-Aided Modeling of Reactive Systems*; Wiley: New York, 2008; pp 95-133.

(6) Poling, B. E., Prausnitz, J. M., and O'Connell, J. P. *Properties of Gases and Liquids*; McGraw-Hill: New York, 2001; pp 11.5-11.20.

(7) Bhatia, S. K. and Perlmutter D. A random pore model for fluid-solid reactions: I. Isothermal, kinetic control. *AIChE J.* **1980**, *26*, 379-386; *AIChE. J.* **1981**, *27*, 247-254.

(8) Ravel, B. and Newville, M. ATHENA, ARTEMIS, HEPHAESTUS: data analysis for X-ray absorption spectroscopy using IFEFFIT. *J. Synch. Rad.* **2005**, *12*, 537-541.

(9) Liu, Y., Meirer, F., Williams, P. A., Wang, J., Andrews, J. C., and Pianetta, P. TXM-Wizard: a program for advanced data collection and evaluation in full-field transmission X-ray microscopy. *J. Synch. Rad.* **2012**, *19*, 281–287.

(10) Weng, T.-C., Waldo G. S., and Penner-Hahn J. E. A method for normalization of X-ray absorption spectra. *J. Synch. Rad.* **2005**, *12*, 506-510.